Atmos. Chem. Phys. Discuss., 15, 9173–9202, 2015
www.atmos-chem-phys-discuss.net/15/9173/2015/
doi:10.5194/acpd-15-9173-2015

Atmospheric Chemistry and Physics
Discussions
Open Access

Stratospheric geoengineering impacts on El Niño/Southern Oscillation

C. J. Gabriel and A. Robock

Department of Environmental Sciences, Rutgers University, New Brunswick, NJ, USA

Received: 2 March 2015 – Accepted: 6 March 2015 – Published: 27 March 2015

Correspondence to: C. J. Gabriel (cjgabriel7@gmail.com)

Published by Copernicus Publications on behalf of the European Geosciences Union.

Abstract

To examine the impact of proposed stratospheric geoengineering schemes on the amplitude and frequency of El Niño/Southern Oscillation (ENSO) variations we examine climate model simulations from the Geoengineering Model Intercomparison Project (GeoMIP) G1–G4 experiments. Here we compare tropical Pacific behavior under anthropogenic global warming (AGW) using the representative concentration pathway resulting in 4.5 $W m^{-2}$ radiative forcing at the end of the 21st Century, the RCP4.5 scenario, with that under G1–G4 and under historical model simulations. Climate models under AGW project relatively uniform warming across the tropical Pacific over the next several decades. We find no statistically significant change in ENSO frequency or amplitude under stratospheric geoengineering as compared with those that would occur under ongoing AGW.

1 Introduction

1.1 Background

The warming of Earth in the Industrial Age is unequivocal, and it is extremely likely that the warming since 1950 is primarily the result of anthropogenic emission of heat trapping gases rather than natural climate variability (IPCC, 2013). Ice core records from the European Project for Ice Coring in Antarctica (EPICA) reveal that current concentrations of the heat trapping gases carbon dioxide and methane are higher now than at any time during the past 650 000 years. (Siegenthaler et al., 2005). All realistic emissions scenarios utilized in the Intergovernmental Panel on Climate Change (IPCC) Fifth Assessment Report reveal that the modeled global mean temperature in 2100 will exceed the full distribution of global mean temperature in proxy reconstructions of global temperature over the past 11 300 years of the Holocene (Marcott et al., 2013).

ACPD
15, 9173–9202, 2015

Ongoing warming is unprecedented in human history both in magnitude and rate of change.

The realization that weathering the impacts of this warming may be beyond human adaptive capacity has generated many proposed mitigation techniques, which focus on limiting emission or increasing storage of heat-trapping gases such as carbon dioxide. Implementation costs and economic, political and societal factors limit societies' will and ability to impose mitigation measures. This has forced recent consideration of geoengineering – intentional manipulation of global-scale physical processes (Crutzen, 2006). Specifically, a form of solar radiation management (SRM) known as stratospheric geoengineering has been proposed. Annual sulfate injections into the tropical stratosphere have the potential to create a long-lasting, well-mixed sulfate aerosol layer, which could reduce incoming shortwave radiation, in an attempt to offset the warming by the excess heat-trapping gases (Robock, 2008). The cost of implementing stratospheric geoengineering is most likely not prohibitive (Robock et al., 2009). Any decision about the implementation would likely be based on substantive issues of risk and feasibility of governance (Caldeira et al., 2013).

Assessment of the efficacy and risk profile of stratospheric geoengineering is underway in a series of standardized climate modeling experiments as part of the Geoengineering Model Intercomparison Project (GeoMIP) (Kravitz et al., 2011). Any assessment of the impact of geoengineering on climate must include analysis of how geoengineering could alter patterns of natural climate variability and how geoengineering could change the mean climate state in such a way that natural climate variability would evolve differently in an intentionally-forced world.

1.2 Research question and motivation

Here we seek to examine whether stratospheric geoengineering would have any impact on the frequency or amplitude of El Niño/Southern Oscillation (ENSO). More specifically, will ENSO amplitude and frequency be different under a regime of geoengineering from that in a global warming scenario? ENSO is the most important source of interannual climate variability. Its amplitude, frequency and the attendant teleconnection patterns have critical consequences for global climate patterns (McPhaden, 2006). ENSO exhibits a 2–7 year periodicity with warm (El Niño) and cold (La Niña) events each lasting 9–12 months and peaking during the DJF season.

The possibility of a connection between warm ENSO events subsequent to stratospheric aerosol loading via volcanism has been explored both in proxy records and model simulations. Despite its relative simplicity, the Zebiak–Cane (ZC) model (Zebiak and Cane, 1987) possesses an exceptional ability to describe the coupled ocean–atmosphere dynamics of the tropical Pacific. By forcing ZC with the calculated radiative forcing from each eruption in the past 1000 years, Emile-Geay et al. (2007) showed that El Niño events tend to occur in the year subsequent to major tropical eruptions, including Tambora (1815) and Krakatau (1883). A strong enough cooling by a volcanic event is likely to cause warming in the eastern Pacific over the next one to two years (Mann et al., 2005). The dynamical "ocean thermostat" describes the mechanism underlying differential heating in the eastern and western Pacific. In the presence of a global strong negative radiative forcing, the western Pacific will cool more quickly than the eastern Pacific. This is because the western Pacific mixed layer's heat budget is almost exclusively from solar heating, while, in the east, both horizontal divergence and strong upwelling contribute to the mixed layer heat budget. Therefore, a uniform solar dimming is likely to result in a muted zonal sea surface temperature (SST) gradient across the equatorial tropical Pacific (Clement et al., 1996). A diminished SST gradient promotes a weakening of trade winds, resulting in less upwelling and an elevated thermocline, further weakening the cross-basin SST gradient. This "Bjerknes feedback" describes how muting of the SST gradient brought on by negative radiative forcing alone is exacerbated by ocean–atmosphere coupling (Bjerknes, 1969). Following the initial increase in El Niño likelihood, La Niña event probability peaks in the third year post-eruption (Maher et al., 2015).

Trenberth et al. (1997) placed the likelihood of an ENSO event in a given year at 31 %. Using 200 ZC simulations lasting 1000 years each, Emile-Geay et al. (2008)

ACPD
15, 9173–9202, 2015

showed that the probability of an El Niño event in the year after the simulated volcanic forcing never exceeded 43 % absent negative (volcanic) radiative forcing of greater than $1\,\mathrm{W\,m^{-2}}$, with modeled next year El Niño probabilities clustered around 31 %. Volcanic events with radiative forcing ranging from -1 to $-3.3\,\mathrm{W\,m^{-2}}$ fit into a transition regime, with the number of events approaching or exceeding the 43 % probability maximum. For all modeled volcanic events with radiative forcing exceeding $-3.3\,\mathrm{W\,m^{-2}}$, the probability of a next year El Niño exceeded 43 %. This is a forced regime – negative radiative forcing applied to the ZC model forced El Niño likelihood out of a free regime and into a regime where enhanced variability would be more likely (Emile-Geay et al., 2007). In the transition and forced regimes, increased El Niño amplitude is also simulated following moderate to strong volcanic events.

Geoengineering schemes simulated in current general circulation models (GCMs) introduce long-lasting radiative forcing of the magnitude found in the transition regime. This means that while radiative forcing of that magnitude does not force the probability of a next year El Niño event to exceed the 43 % free oscillation maximum threshold, instead the radiative forcing applied does fit into a range in which the 43 % threshold is exceeded during the next year in some simulations. Therefore, we ask whether solar dimming lasting many years, as a proxy for sulfate injections, or sulfate injections lasting many years as simulated by models may also alter El Niño or La Niña event frequency and amplitude. Rather than using the ZC model, we use various geoengineering experiment designs in modern, state-of-the-art GCMs to determine whether forcing from stratospheric aerosol injections, added continuously, will load the deck in favor of El Niño events in the succeeding year. No modeling study has ever evaluated the impact of long term solar dimming or continuous stratospheric sulfate injections on ENSO.

Since our comparison is between El Niño and La Niña amplitude and frequency under a geoengineering regime and under a scenario of unabated global warming, the evolution of ENSO behavior under global warming, independent of geoengineering, is also of interest. Overwhelming evidence from climate model experiments shows that

ACPD
15, 9173–9202, 2015

C. J. Gabriel and A. Robock

geoengineering could effectively reduce or offset the surface temperature increase resulting from global warming by limiting the amount of incoming shortwave radiation, compensating for global warming (Jones et al., 2013; Robock et al., 2008). An alternative theory for why ENSO amplitude and frequency may be different in the future under a geoengineering regime than under global warming is based on the fact that ENSO events may evolve differently from a warmer tropical Pacific mean state under global warming than if a geoengineering scheme were imposed.

Kirtman and Schopf (1998) showed that tropical Pacific mean-state changes on decadal timescales are more responsible than atmospheric noise for changes in ENSO frequency and predictability. This does not imply any external cause for the changes in ENSO, but does imply that a uniform warming of the tropical Pacific may cause changes in ENSO. Despite the lack of a robust multi-model ENSO signal in the Coupled Model Intercomparison Project 5 (CMIP5) models (Taylor et al., 2012), there are suggestions that strong El Niño events may become far more likely under global warming, specifically in a multi-model ensemble experiment using RCP8.5. As global warming continues, background state tropical Pacific SSTs are expected to warm faster along the equator than off the equator, and faster in the east than in the west – the inverse of the ocean dynamical thermostat mechanism (Held et al., 2010). With the weaker zonal SST gradient in the tropical Pacific, there will be more occurrences of higher SSTs in the eastern Pacific, promoting large scale organization of convection further to the east, with twice as many strong El Niño events over 2000 years of RCP8.5 runs (Cia et al., 2014). We will not seek to replicate the RCP8.5 results. No physically plausible geoengineering experiment would seriously attempt to offset RCP 8.5 with solar dimming or sulfate injections. Therefore, we use RCP4.5 as the control in GeoMIP experiments, and will attempt to identify if the long term mean state changes generate divergent ENSO frequency under geoengineering and global warming.

1.3 Representation of the Tropical Pacific in CMIP

The ability to detect subtle differences in the tropical Pacific under global warming vs. geoengineering requires sufficiently skilled models. Proper depiction of ENSO in a GCM is confounded by the fact that ENSO is a coupled ocean-atmospheric phenomenon, generated by the interaction of many processes, each occurring on one of several different time scales. Nearly all CMIP3 models were able to produce an ENSO cycle, but significant errors were evident (Guilyardi et al., 2009). Analysis of CMIP5 models has shown significant improvement, but the improvement has not been revolutionary. Such a comparison is facilitated by standardized "metrics developed within the CLIVAR (Climate and Ocean: Variability, Predictability and Change) Pacific Panel that assess the tropical Pacific mean state and interannual variability" (Bellenger et al., 2013). The following metrics were used in the CLIVAR CMIP3/CMIP5 comparison: ENSO amplitude, structure, spectrum and seasonality. Some process-based variables were also studied, including the Bjerknes feedback.

Key results included that 65 % of CMIP5 models produce ENSO amplitude within 25 % of observations as compared to 50 % for CMIP3. Other results included improved seasonal phase-locking and the proper spatial pattern of SSTs at the peak of ENSO events. Despite the improvement in these result-based variables, analysis of process-based variables, such as the Bjerknes feedback, showed less consistent improvement. This gives rise to the possibility that the bottom-line improvement in ENSO depiction was at least partially the result of error cancellation, rather than clear improvements in parameterization and simulation of physical processes (Yeh et al., 2012; Guilyardi et al., 2012; Bellenger et al., 2013). A particularly striking area of divergence between modeling and observations is in the absence of a shift from a subsidence regime to a convective regime in the equatorial central Pacific during evolution of El Niño events. Many models maintained a subsidence regime or convective regime at all times over the equatorial central Pacific (Bellenger et al., 2013). This error likely led to the muting

ACPD
15, 9173–9202, 2015

of the negative shortwave feedback in many models, leading to muted damping of ENSO events in those models.

Both the improvement in depiction of ENSO amplitude and seasonality from CMIP3 to CMIP5 and the ability to understand the simulation of key process-based variables motivate an analysis of ENSO and geoengineering using CMIP5 GCMs.

2 Methods

In this experiment, output from nine GeoMIP-participating GCMs, each running between one and three ensemble members, of each experiment G1–G4 are analyzed. These GeoMIP experiments are described by Kravitz et al. (2011). See Fig. 1 for schematics of GeoMIP experiments G1–G4 and Tables 1 and 2 for details about the GCMs used in these experiments. The G1 experiment – instantaneous quadrupling of CO_2 coupled with a concurrent fully offsetting reduction of the solar constant – was designed to elicit robust responses, which then facilitate elucidation of physical mechanisms for further analysis. We compared G1 output to a control run in which the atmospheric carbon dioxide concentration is instantaneously quadrupled. The G2 experiment combines a 1 % $year^{-1}$ CO_2 increase with a fully offsetting reduction in the solar constant. The G3 experiment combines RCP4.5 with a fully offsetting sulfur dioxide injection. The G4 experiment – stratospheric loading of 25 % the SO_2 mass of the 1991 Mt. Pinatubo volcanic eruption (5 Tg) each year concurrent with RCP4.5, with top-of-atmosphere radiation balance not fixed at zero – attempts to replicate a physically and politically plausible large scale geoengineering deployment scenario. G3 and G4 output were compared to an RCP4.5 control and all experiments G1–G4 were compared to observations and historical models from a control period, 1966–2005. The ability to analyze such a large amount of climate model output is why we decided to use all four GeoMIP experiments. ENSO signals are subtle and best deciphered from a large sample.

To identify and analyze ENSO variability and amplitude, absent the contamination of the signal induced in the immediate aftermath of application of initial solar dimming or stratospheric aerosol forcing, the first 10 years of each geoengineering model run were removed. The relevant comparison periods become either "Years 11–50" in G1 and 2030–2069 in G2–G4. Initial forcing is applied in "Year 1" in G1 and in 2020 in G2–G4. This 40-year interval is then compared to RCP4.5 2030–2069 and historical 1966–2005 for each respective model and to observations. We used the Kaplan (1998) SST data set because it is well-documented and used in many of the referenced papers. Differences between the Kaplan data and other available data sets are trivial during the period of data used.

We used several SST-based indices to quantify the amplitude and phase of the ENSO cycle. For each ensemble member of each model, a time series of the Niño 3.4 index was generated. We choose Niño 3.4 over Niño 3 or Niño 4 because we find that the Niño 3.4 region remains the center of action for ENSO variability both in observations and models. The Niño 3.4 region is the area 120–170° W and 5° N–5° S. The Niño 3 region misses a good deal of the Modoki ENSO-type variability, while Niño 4 misses a good deal of canonical ENSO-type variability. We define an ENSO event as a departure of the 5-month running mean Niño 3.4 index (computed over 5° S–5° N, 120–170° W) of greater than 0.5 K from the 2030–2069 climatology, with the linear trend removed from the 2030–2069 climatology before anomalies are calculated. This anomaly must persist for more than five months to qualify as an ENSO event. Cold and warm events have the same definition, just with opposite sign. Anomalies in the historical data and the observational record are calculated relative to a 1966–2005 climatology, which is also detrended before anomalies are calculated. G1 output is analyzed absent detrending, as there is no trend in the data.

We used skin temperature (T_S) anomalies rather than SST anomalies to build the Niño 3.4 time series for the BNU, IPSL and MPI, and models, because they were available on a regular grid. For the purpose of computing an anomaly-based index, the variable T_S is an excellent SST proxy variable, which is interchangeable with SST. In

ACPD
15, 9173–9202, 2015

addition to looking at variables that describe surface temperature anomalies, we considered the Southern Oscillation Index (SOI), which is a standardized index based on the atmospheric pressure difference between Darwin, Australia, and Tahiti, because climate change does not produce SOI trends, except for a trivial increase as a result of increased water vapor concentration in a warmer world. Ideally, using SOI as a proxy for SST or T_S would allow inspection of the data absent the complications of dealing with a trend. Unfortunately SOI simulations show drastically muted variability when compared with SST and T_S based indexes in the GCMs. Figure 2 shows a spatial comparison between observed SOI-SST correlation and that modeled in a representative GISS historical run spanning the same time interval as the observations, and Fig. 3 for corresponding time series. These examples are representative of the other GCMs, and therefore, the results of the SOI analysis were not used in our study.

Presently the National Oceanic and Atmospheric Administration Climate Prediction Center defines the climatological base period from which we calculate the departure from the current value and define an ENSO event as 1981–2010. We depart from this definition due to the robust warming trend in tropical SST in the Pacific both during the 1966–2005 comparison, and in 2030–2069 model runs, which show continued warming of the tropical Pacific. The detrended 40-year average produces a more realistic assessment of the base climate from which a particular ENSO event would evolve. This avoids the trap of identifying spurious ENSO events toward the end of the time series, which are really artifacts of the warming trend. Ideally, a climatological period in a rapidly changing climate would span less than 40 years. However, longer term natural trends in Pacific SST variability, including extended ENSO warm or cold periods, force use of a lengthy climatological base period to avoid comparing variability against a climatology that also includes that same variability.

The ENSO parameters evaluated are amplitude and frequency. El Niño amplitude is defined here as the peak anomaly value (in K) found during each El Niño event in the time series. La Niña amplitude is defined here as the mean negative peak anomaly value (in K) found during each ENSO event in the time series. Frequency is counted as the number of warm and cold events in each 40-year time slice. These parameters are chosen because ENSO frequency and amplitude have particular importance as global climate drivers.

The ENSO frequency and amplitude calculated in each ensemble member of each experiment (G1–G4) are compared (1) to other ensemble members from the same model for the same experiment, if available, (2) to their respective control runs, (3) to runs from other models with the same experimental design and (4) with different experimental designs, (5) to historical model runs, and (6) to observations. From this we seek to identify significant differences between model output from geoengineering scenarios, global warming, and historical runs compared to each other and to observations, as well as differences between models running the same G1–G4 experiment. Not only do we seek to analyze differences in ENSO amplitude and frequency between different scenarios, but we also seek to identify ENSO tendencies specific to particular models. The discussion below includes the successes and limitations of CMIP5 GCMs in depicting ENSO.

3 Results

3.1 Data excluded from final comparison

Although great strides have been made in the modern GCMs' ability to depict a realistic ENSO cycle, not all models are yet able to simulate a realistic ENSO cycle. Prior to further analysis, we applied two simple amplitude-based filters to exclude unreasonable ENSO time series data. The BNU-ESM output was excluded, because runs from more than one of several experiments found unrealistic 40-year ENSO time series where the substantial portion of warm and cold events maximum amplitude exceeded 3 K. Some BNU-ESM events exceeded 4 K, nearly a factor of 2 greater than the largest amplitude warm or cold events in the observational record. The model also produced nearly annual swings from implausibly strong warm events to cold events and back, implying an almost constant non-neutral state (Fig. 4).

The MIROC-ESM and MIROC-ESM-CHEM output were also both excluded. Runs from more than one experiment in those models resulted in unrealistic 40-year ENSO time series without a single positive anomaly of more than 1 K of the Niño 3.4 Index. Negative anomalies were similarly suppressed in simulations from both models (Fig. 5).

3.2 Analysis

We considered output from six GeoMIP participating GCMs: CanESM, CSIRO, GISS, HadGEM, IPSL and MPI (Tables 1 and 2). Before making comparisons between models for experiments, we first aggregated all of the runs: all ensemble members from all experiments over each respective 40-year time slice. We find strong agreement between all aggregated model data and the observations, with 9 warm events, 8 cold events and a maximum warm amplitude of 2.3 K and maximum cold amplitude of 1.9 K in the 1966–2005 observational record, and an average of 8.1 warm events, 8.3 cold events, a maximum warm amplitude of 1.7 K and a maximum cold amplitude of 1.8 K as the average for all models. Therefore, in this subset of GeoMIP CMIP5 models, the number of warm events, cold events, warm amplitude and cold amplitude are similar to that seen in observations, although there is a large spread within each model and between models.

The first comparison between model runs is between all GeoMIP G1–G4 runs from 2030–2069 and all non-GeoMIP runs over the same time interval, because each group – GeoMIP and non-GeoMIP – is a relatively large sample size relative to the direct experiment to control comparisons. An average of 8.11 warm events and 8.32 cold events occur during the 40-year period in the 47 GeoMIP members. An average of 7.89 warm and 7.97 cold events occur in the 37 non-GeoMIP runs (Fig. 6). The mean maximum warm event amplitude in the GeoMIP runs is 1.66 K (1.71 K non-GeoMIP) and the cold event maximum amplitude is 1.76 K (1.72 K non-GeoMIP) (Fig. 7). Differences in the two data sets – GeoMIP vs. non-GeoMIP – are not significant

ACPD
15, 9173–9202, 2015

Stratospheric geoengineering impacts on ENSO

C. J. Gabriel and A. Robock

Next, we compare all GeoMIP runs against all RCP4.5 runs. This also generates no statistically significant results. An average of 8.38 warm and 8.67 cold events occur in the 21 RCP4.5 runs. The maximum warm event amplitude is 1.90 K and the maximum cold event amplitude is 1.81 K in the RCP4.5 runs. Both the maximum warm amplitude and the maximum cold amplitude in the RCP4.5 run average are higher than the average of any of the G1–G4 experiment ensembles. Additionally, the frequency of warm events and the amplitude of both warm and cold events is higher in the average of all historical model runs than in any of the G1–G4 experiment ensembles means. (Figs. 7 and 9).

Only two of our comparisons yield statistically significant results at a 95 % confidence level. 2030–2069 RCP4.5 warm event frequency is less than warm event frequency in 1966–2005 historical model runs. Also, cold event frequency is higher in an ensemble of G1 and G2 runs than it is in an ensemble of abrupt four times CO_2 and 1 % yr^{-1} CO_2 increase runs. Taken together, these results may suggest that ENSO events will be less frequent in a world with a warmer tropical Pacific mean state when compared to the relatively cool tropical pacific of the recent past or that of a geoengineered world.

3.3 Comparisons between models

Disagreement between models was far more significant than that between different experiments or scenarios. This is unsurprising given the wide range of ENSO predictions among CMIP5 models. One of the features most readily apparent across all models was the lack of coupling between the ocean and the atmosphere in the eastern Pacific. The ENSO center of action was confined to a small area in the central Pacific, whereas the ocean–atmosphere coupling was strong across the equatorial eastern extent of the basin in the observational record (Fig. 2).

Next we make model vs. model comparisons – comparing all ensemble members of runs from each model against each other (see Figs. 8 and 9 for ENSO event amplitude and frequency simulated by each model). Of the models not excluded, the CanESM results diverged far more than the other models from the overall mean on all four pa-

ACPD
15, 9173–9202, 2015

rameters evaluated. CanESM depicts ENSO warm and cold events that are both more frequent and stronger than that documented in the Kaplan SST observational record. The CanESM is also significantly different (99 % confidence) from the five other models on all four parameters, only showing agreement with the MPI on one parameter: cold event amplitude. The CSIRO model depicts the lowest number of both cold and warm events, as well as event amplitudes that are on the low end. The GISS, HadGEM, IPSL and MPI models are not in close agreement on all four parameters, but they agree more than the CSIRO and CanESM. The best agreement between models existed between the HadGEM and IPSL, which agreed on all but cold event amplitude.

4 Discussion

It is unclear if or how ENSO event frequency or amplitude in a geoengineered world will differ from the observational record, historical model runs, or under global warming. However, by evaluating GeoMIP output, and comparing it to modeled non-geoengineering scenarios, we learn several things. First, not all models depict a realistic enough ENSO cycle to be included in the analysis. For example, a representative BNU G1 run showed a cold event with a maximum anomaly of −4.8 K during a relatively short duration La Niña event. Similar non-geoengineering runs revealed equally extreme amplitude and short lasting events. The observational record fails to hint that such an event has occurred, and none of the other models simulate anything like such an event. Future work could explore why simulated BNU ENSO events are so strong, short and frequent relative to observations and other models.

Second, even those models that simulate a physically plausible ENSO cycle show statistically significant differences in amplitude and or frequency. Additionally, models generally depict less robust warm and cold event amplitude than what is seen in observations. The agreement between several of the models included – GISS, IPSL, HadGEM and MPI – was quite good. However, they consistently model both fewer warm and cold events and lower warm and cold event amplitudes than seen in obser-

ACPD
15, 9173–9202, 2015

vations or in the historical runs. CLIVAR's analysis of process-based variables in CMIP 3/5 – which quantify a GCM's ability to simulate key ENSO processes – is underway. That work is more squarely focused at determining exactly how the simulation of both ENSO events and the underlying ENSO processes can be improved in GCMs.

Both warm and cold event frequency is generally similar between geoengineering experiments and their respective controls. Although neither the comparison between GeoMIP and non-GeoMIP output, nor the comparison of G3/G4 output with RCP4.5 output showed statistically significant differences at a 95 % confidence level, there are differences worthy of discussion. In particular, models that instantaneously quadrupled carbon dioxide showed substantially muted ENSO in the period between 10 and 50 years after the quadrupling, with an average of 6.43 warm events and 6.71 cold events in that period. The G1 run, which quadruples carbon dioxide, but also fully offsets with the solar constant reduction, shows about 8.7 warm and cold events in each. Maximum amplitude was about the same for each. This could suggest that more extreme global warming scenarios may suppress ENSO variability. One interesting, and statistically significant result was that RCP4.5 warm event frequency was significantly suppressed ((95 % confidence) compared with historical simulations. This has no bearing on geoengineering, but it suggests diminished ENSO frequency relative to historical model runs in an RCP4.5 world. Lastly, the spread of warm and cold event frequency and warm or cold event amplitude among ensemble members performing the same run is large. All of these factors are challenges in comparing ENSO frequency and amplitude in a geoengineered world, as compared to a global warming world. Although we do not identify a robust ENSO signal in the geoengineering experiments, future model improvement and more impact-directed process based analysis of tropical Pacific variability may reveal subtle differences in ENSO behavior under modeled geoengineering regimes in the future.

Acknowledgements. We thank all the climate modeling groups for conducting the GeoMIP simulations and making their output available. We thank B. Kravitz for his overall leadership of GeoMIP. This work is supported by NSF grants AGS-1157525 and GEO-1240507.

ACPD
15, 9173–9202, 2015

References

Arora, V. K., Scinocca, J. F., Boer, G. J., Christian, J. R., Denman, K. L., Flato, G. M., Kharin, V. V., Lee, W. G., and Merryfield, W. J.: Carbon emission limits required to satisfy future representative concentration pathways of greenhouse gases, Geophys. Res. Lett., 38, L05805, doi:10.1029/2010GL046270, 2011.

Bellenger, H., Guilyardi, E., Leloup, J., Lengaigne, M., and Vialard, J.: ENSO representation in climate models: from CMIP3 to CMIP5, Clim. Dynam., 42, 1999–2018, 2013.

Bjerknes, J.: Atmospheric teleconnections from the equatorial Pacific, Mon. Weather Rev., 97, 163–172, 1969.

Caldeira, K., Bala, G., and Cao, L.: The science of geoengineering, Annu. Rev. Earth Pl. Sc., 41, 231–256, 2013.

Cai, W., Wang, G., Santoso, A., McPhaden, M., Wu, L., Jin, F.-F., Timmermann, A., Collins, M., Vecchi, G., Lengaigne, M., England, M., Dommenget, D., Takahashi, K., and Guilyardi, E.: Increasing frequency of extreme El Niño events due to greenhouse warming, Nat. Climate Change, 4, 111–116, 2014.

Clement, A. C., Seager, R., Cane, M. A., and Zebiak, S. E.: An ocean dynamical thermostat, J. Climate., 9, 2190–2196, 1996.

Collins, W. J., Bellouin, N., Doutriaux-Boucher, M., Gedney, N., Halloran, P., Hinton, T., Hughes, J., Jones, C. D., Joshi, M., Liddicoat, S., Martin, G., O'Connor, F., Rae, J., Senior, C., Sitch, S., Totterdell, I., Wiltshire, A., and Woodward, S.: Development and evaluation of an Earth-System model – HadGEM2, Geosci. Model Dev., 4, 1051–1075, doi:10.5194/gmd-4-1051-2011, 2011.

Crutzen, P.: Albedo enhancement by stratospheric sulfur injections: a contribution to solve a policy dilemma?, Climatic Change, 77, 211–219, 2006.

Dai, Y., Zeng, X. B., Dickinson, R. E., Baker, I., Bonan, G. B., Bosilovich, M. G., Denning, A. S., Dirmeyer, P. A., Houser, P. R., Niu, G. Y., Oleson, K. W., Schlosser, C. A., and Yang, Z. L.: The Common Land Model (CLM), B. Am. Meteorol. Soc., 84, 1013–1023, 2003.

Dufresne, J. L., Foujols, M. A., Denvil, S., Caubel, A., Marti, O., Aumont, O, Balkanski, Y., Bekki, S., Bellenger, H., Benshila, R., Bony, S., Bopp, L., Braconnot, P., Brockmann, P., Cadule, P., Cheruy, F., Codron, F., Cozic, A., Cugnet, D., de Noblet, N., Duvel, J. P., Ethé, C., Fairhead, L., Fichefet, T., Flavoni, S., Friedlingstein, P., Grandpeix, J. Y., Guez, L., Guilyardi, E., Hauglustaine, D., Hourdin, F., Idelkadi, A., Ghattas, J., Joussaume, S., Kageyama, M., Krinner, G., Labetoulle, S., Lahellec, A., Lefebvre, M. P., Lefevre, F., Levy, C., Li, Z. X., Lloyd, J., Lott, F., Madec, G., Mancip, M., Marchand, M., Masson, S., Meurdesoif, Y., Mignot, J., Musat, I., Parouty, S., Polcher, J., Rio, C., Schulz, M., Swingedouw, D., Szopa, S., Talandier, C., Terray, P., Viovy, N., and Vuichard, N.: Climate change projections using the IPSL-CM5 Earth System Model: from CMIP3 to CMIP5, Clim. Dynam., 40, 2123–2165, 2013.

Emile-Geay, J., Seager, R., Cane, M. A., Cook, E. R., and Haug, G. H.: Volcanoes and ENSO over the past millennium, J. Climate, 21, 3134–3148, 2007.

Giorgetta, M. A., Jungclaus, J. H., Reick, C. H., Legutke, S., Bader, J., Böttinger, M., Brovkin, V., Crueger, T., Esch, M., Fieg, K., Glushak, K., Gayler, V., Haak, H., Hollweg, H.-D., Ilyina, T., Kinne, S., Kornblueh, L., Matei, D., Mauritsen, T., Mikolajewicz, U., Mueller, W. A., Notz, D., Pithan, F., Raddatz, T., Rast, S., Redler, R., Roeckner, E., Schmidt, H., Schnur, R., Segschneider, J., Six, K., Stockhause, M., Timmreck, C., Wegner, J., Widmann, H., Wieners, K.-H., Claussen, M., Marotzke, J., and Stevens, B.: Climate and carbon cycle changes from 1850 to 2100 in MPI-ESM simulations for the coupled model intercomparison project phase 5, J. Adv. Mode. Earth Sys., 5, 572–597, 2013.

Guilyardi, E., Wittenberg, A., Fedorov, A., Collins, M., Wang, C., Capotondi, A., Oldenborgh, G. J. V., and Stockdale, T.: Understanding El Niño in ocean–atmosphere general circulation models: progress and challenges, B. Am. Meteorol. Soc., 90, 325–340, 2009.

Guilyardi, E., Bellenger, H., Collins, M., Ferrett, S., Cai, W., and Wittenberg, A.: A first look at ENSO in CMIP5, CLIVAR Exchanges, 58, 29–32, 2012.

Held, I. M., Winton, M., Takahashi, K., Delworth, T., Zeng, F., and Vallis, G. K.: Probing the fast and slow components of global warming by returning abruptly to preindustrial forcing, J. Climate, 23, 2418–2427, 2010.

IPCC: Summary for policymakers, in: Climate Change, 2013: The Physical Science Basis. Contribution of Working Group I to the 5th Assessment Report of the Intergovernmental Panel on Climate Change, Cambridge University Press, Cambridge, UK and New York, NY, USA, 1–30, 2013.

Jones, A., Haywood, J., Boucher, O., Kravitz, B., and Robock, A: Geoengineering by stratospheric SO_2 injection: results from the Met Office HadGEM2 climate model and comparison with the Goddard Institute for Space Studies ModelE, Atmos. Chem. Phys., 10, 5999–6006, doi:10.5194/acp-10-5999-2010, 2010.

Kirtman, B. P. and Schopf, P. S.: Decadal variability in ENSO predictability and prediction, J. Climate, 11, 2804–2822, 1998.

Kravitz, B., Robock, A., Boucher, O., Schmidt, H., Taylor, K. E., Stenchikov, G., and Schulz, M.: The geoengineering model intercomparison project (GeoMIP), Atmos. Sci. Lett., 12, 162–167, 2011.

Maher, N., McGregor, S., England, M. H., and Gupta, A. S.: Effects of volcanism on Tropical variability, Geophys. Res. Lett. (submitted), 2015.

Mann, M. E., Cane, M. A., Zebiak, S. E., and Clement, A.: Volcanic and solar forcing of the Tropical Pacific over the past 1000 years, J. Climate, 18, 447–456, 2005.

Marcott, S. A., Shakun, J. D., Clark, P. U., and Mix, A. C.: A reconstruction of regional and global temperature for the past 11 300 years, Science, 339, 1198–1201, 2013.

McPhaden, M. L., Zebiak, S. E., and Glantz, M. H.: ENSO as an integrating concept in earth science, Science, 314, 1739–1745, 2006.

Phipps, S. J., Rotstayn, L. D., Gordon, H. B., Roberts, J. L., Hirst, A. C., and Budd, W. F.: The CSIRO Mk3L climate system model version 1.0 – Part 1: Description and evaluation, Geosci. Model Dev., 4, 483–509, doi:10.5194/gmd-4-483-2011, 2011.

Phipps, S. J., Rotstayn, L. D., Gordon, H. B., Roberts, J. L., Hirst, A. C., and Budd, W. F.: The CSIRO Mk3L climate system model version 1.0 — Part 2: Response to external forcings, Geosci. Model Dev., 5, 649–682, doi:10.5194/gmd-5-649-2012, 2012.

Robock, A.: Whither geoengineering?, Science, 320, 1166–1167, 2008.

Robock, A., Marquardt, A., Kravitz, B., and Stenchikov, G.: The benefits, risks, and costs of stratospheric geoengineering, Geophys. Res. Lett., 36, L19703, doi:10.1029/2009GL039209, 2009.

Schmidt, G. A., Ruedy, R., Hansen, J. E., Aleinov, I., Bell, N., Bauer, M., Bauer, S., Cairns, B., Canuto, V., Cheng, Y., Del Genio, A., Faluvegi, G., Friend, A. D., Hall, T. M., Hu, Y., Kelley, M., Kiang, N. Y., Koch, D., Lacis, A. A., Lerner, J., Lo, K. K., Miller, R. L., Nazarenko, L., Oinas, V., Perlwitz, J. P., Perlwitz, J., Rind, D., Romanou, A., Russell, G. L., Sato, M., Shindell, D. T., Stone, P. H., Sun, S., Tausnev, N., Thresher, D., and Yao, M. S.: Present-day atmospheric simulations using GISS ModelE: comparison to in situ, satellite and reanalysis data, J. Climate, 19, 153–192, 2006.

Siegenthaler, U., Stocker, T. F., Monnin, E., Luthi, D., Schwander, J., Stauffer, B., Raynaud, D., Barnola, J. M., Fischer, H., Masson-Delmotte, V., and Jouzel, J.: Stable carbon cycle-climate relationship during the late Pleistocene, Science, 310, 1313–1317, 2005.

Taylor, K. E., Stouffer, R. J., and Meehl, G.A.: An overview of CMIP5 and the experiment design, B. Am. Meteorol. Soc., 93, 485–498, doi:10.1175/BAMS-D-11-00094.1, 2012.

ACPD
15, 9173–9202, 2015

Stratospheric geoengineering impacts on ENSO

C. J. Gabriel and A. Robock

Tilmes, S., Fasullo, J., Lamarque, J. F., Marsh, D. R., Mills, M., Alterskjær, K., Muri, H., Kristjánsson, J. E., Boucher, O., Schulz, M., Cole, J. N. S., Curry, C. L., Jones, A., Haywood, J., Irvine, P. J., Ji, D., Moore, J. C., Karam, D. B., Kravitz, B., Rasch, P. J., Singh, B., Yoon, J.-H., Niemeier, U., Schmidt, H., Robock, A., Yang, S., and Watanabe, S.: The hydrological impact of geoengineering in the Geoengineering Model Intercomparison Project (GeoMIP), J. Geophys. Res.-Atmos., 118, 11036–11058, 2013.

Trenberth, K. E. and Hoar, T. J.: El Niño and climate change, Geophys. Res. Lett., 24, 3057–3060, 1997.

Watanabe, S., Hajima, T., Sudo, K., Nagashima, T., Takemura, T., Okajima, H., Nozawa, T., Kawase, H., Abe, M., Yokohata, T., Ise, T., Sato, H., Kato, E., Takata, K., Emori, S., and Kawamiya, M.: MIROC-ESM 2010: model description and basic results of CMIP5-20c3m experiments, Geosci. Model Dev., 4, 845–872, doi:10.5194/gmd-4-845-2011, 2011.

Yeh, S. W., Ham, Y.-G., and Lee, J.-Y.: Changes in the tropical Pacific SST trend from CMIP3 to CMIP5 and its implication of ENSO, J. Climate, 25, 7764–7771, 2012.

Zebiak, S. E. and Cane, M. L.: A model El Niño/Southern Oscillation, Mon. Weather Rev., 115, 2262–2278, 1987.

ACPD
15, 9173–9202, 2015

Stratospheric geoengineering impacts on ENSO

C. J. Gabriel and A. Robock

Table 1. The names of the climate models used in this study, with short names and references. Asterisks indicate that the models were excluded from comparison due to unrealistic ENSO variability.

Model	Model short name	Reference
*BNU-ESM	BNU	Dai et al. (2003)
CanESM2	CanESM	Arora et al. (2011)
CSIRO-Mk3L	CSIRO	Phipps et al. (2011, 2012)
GISS-E2-R	GISS	Schmidt et al. (2006)
HadGEM2-ES	HadGEM	Collins et al. (2011)
IPSL-CM5A-LR	IPSL	Dufresne et al. (2012)
*MIROC-ESM	MIROC	Watanabe et al. (2011)
*MIROC-ESM-CHEM	MIROC-C	Watanabe et al. (2011)
MPI-ESM-LR	MPI	Giorgetta et al. (2012)

ACPD
15, 9173–9202, 2015

Stratospheric geoengineering impacts on ENSO

C. J. Gabriel and A. Robock

Table 2. Models analyzed in each experiment. Asterisks indicate that the models were excluded from comparison due to unrealistic ENSO variability. The number of ensemble members for each experiment is given in parenthesis after the model name.

a. Models in G1	b. Models in G2
*BNU-ESM (2)	*BNU-ESM (3)
CanESM2 (3)	CanESM2 (3)
CSIRO-Mk3L (3)	CSIRO-Mk3L (3)
GISS-E2- (3)	GISS-E2-R] (3)
HadGEM2-ES (1)	HadGEM2-ES (3)
IPSL-CM5A-LR (1)	IPSL-CM5A-LR (1)
*MIROC-ESM (1)	*MIROC-ESM (1)
MPI-ESM-LR (1)	MPI-ESM-LR (1)
c. Models in G3	**d. Models in G4**
*BNU-ESM (1)	*BNU-ESM (2)
GISS-E2-R (3)	CanESM2 (3)
HadGEM2-ES (2)	CSIRO-Mk3L (3)
IPSL-CM5A-LR (1)	GISS-E2-R (3)
MPI-ESM-LR (3)	HadGEM2-ES (1)
	IPSL-CM5A-LR (1)
	*MIROC-ESM (1)
	*MIROC-ESM-CHEM (1)
	MPI-ESM-LR (1)

ACPD
15, 9173–9202, 2015

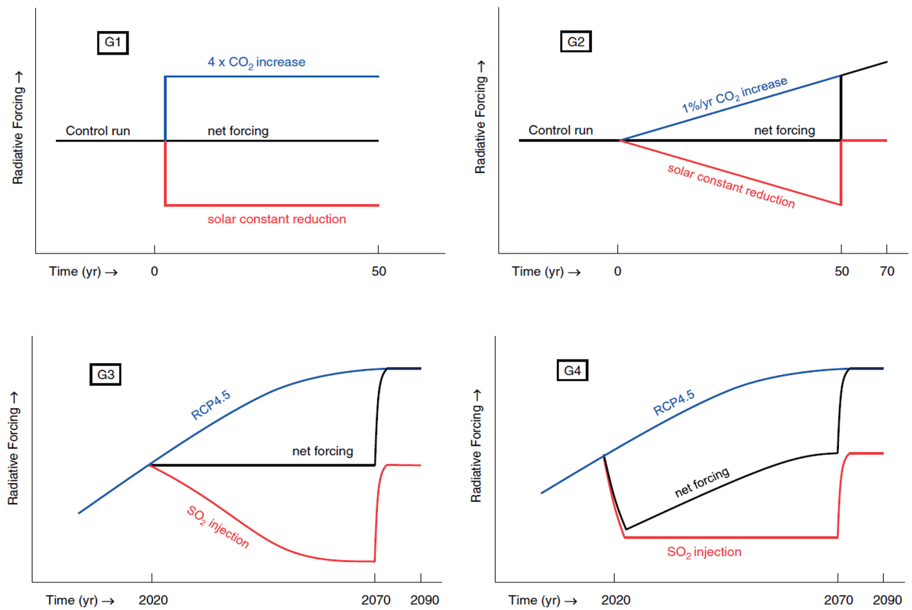

Figure 1. GeoMIP G1–G4 experiment designs. Figures 1–4 from Kravitz et al. (2011).

ACPD
15, 9173–9202, 2015

Stratospheric geoengineering impacts on ENSO

C. J. Gabriel and A. Robock

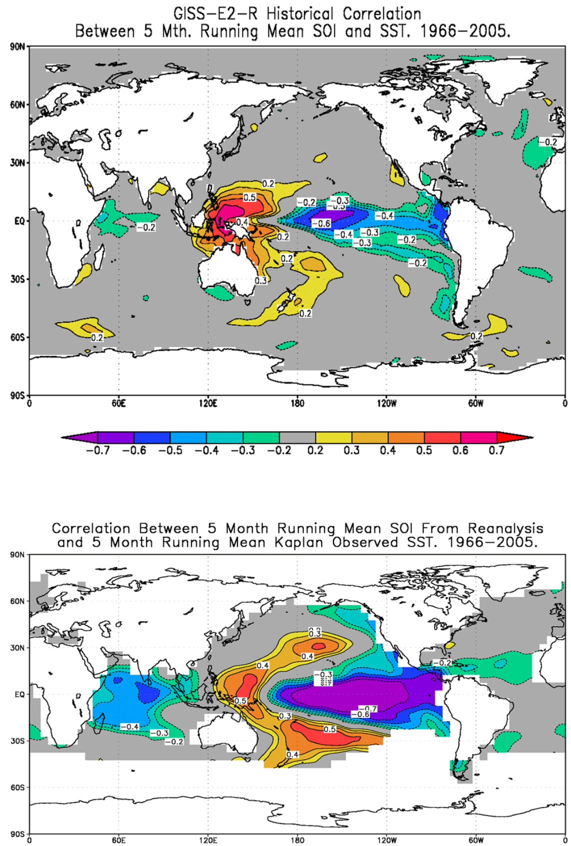

Figure 2. Top panel shows spatial correlation between GISS historical sea surface temperature (SST) and the Southern Oscillation Index (SOI). The area of strong negative correlation is confined to a small region in the central Pacific, relative to the broad area of strong negative correlation in the observations in the bottom panel, which shows the spatial correlation between NCEP SLP reanalysis and the Kaplan (1998) SST observations data set.

ACPD
15, 9173–9202, 2015

C. J. Gabriel and A. Robock

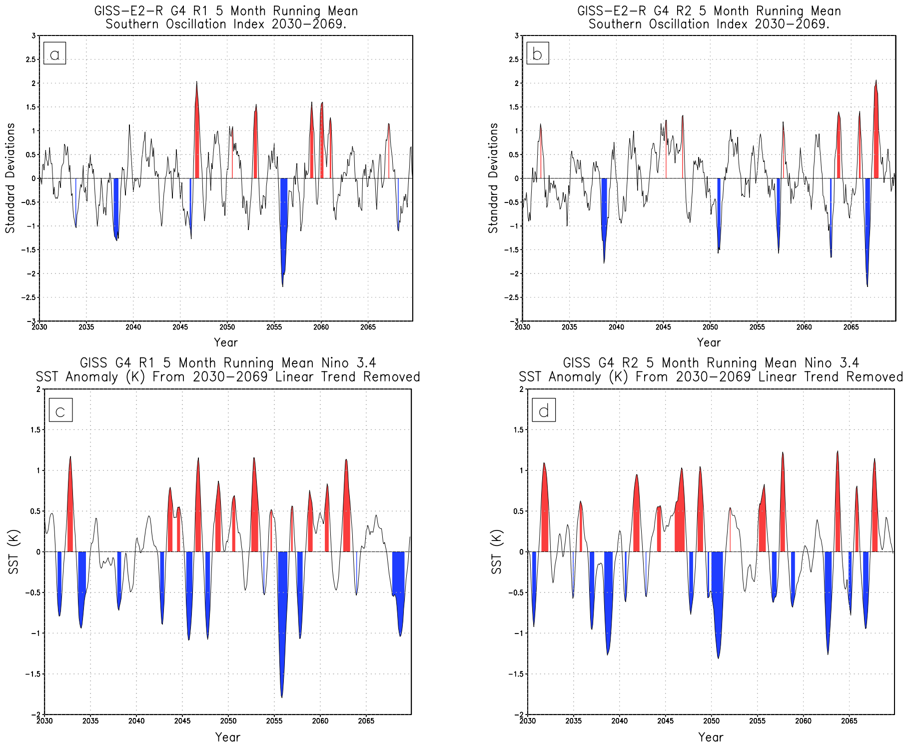

Figure 3. Time series of normalized Southern Oscillation Index (SOI) for **(a)** GISS G4 Run 1 and **(b)** GISS G4 Run 2. In the context of SOI, ENSO events are defined as departures of 0.5 SDs from zero. SOI warm events are highlighted in red, while cold events are highlighted in blue. No highlight is applied during an ENSO neutral phase. Time series of SST in Niño 3.4 region for **(c)** GISS G4 Run 1 and **(d)** GISS G4 Run 2. The SST-based index in the bottom panels depicts more realistic ENSO variability, and therefore SOI is not used as an SST proxy.

ACPD
15, 9173–9202, 2015

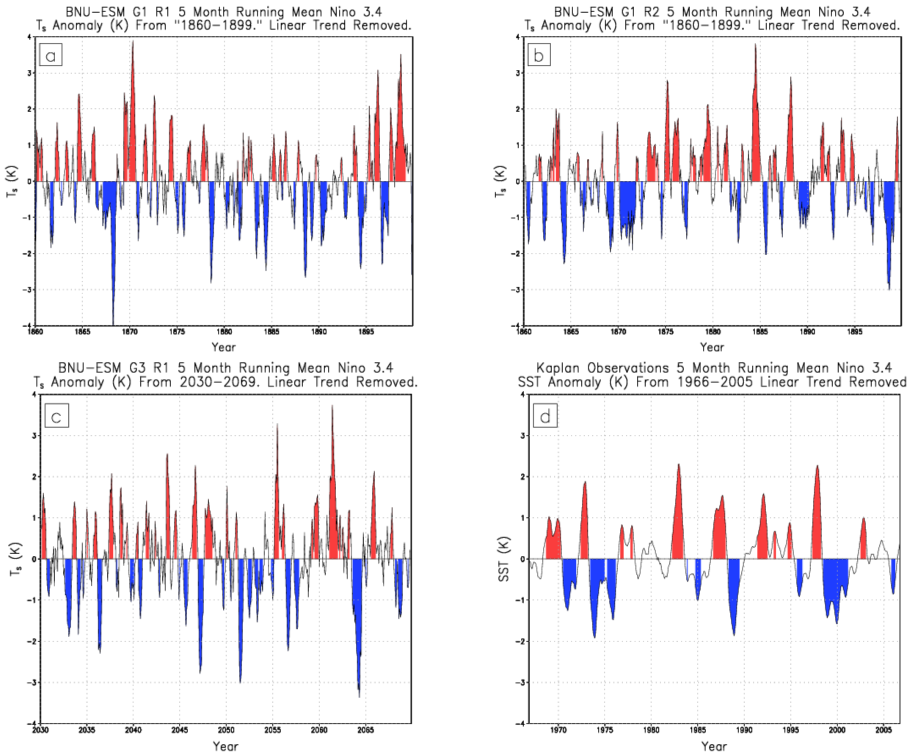

Figure 4. Time series of Niño 3.4 anomalies from three experimental runs, **(a)** G1 run 1, **(b)** G1 run 2, and **(c)** G3 run 1, of the BNU-ESM model compared to observations **(d)**. Red coloring indicates ENSO warm events, while blue shading indicates ENSO cold events. The model is excluded due to unrealistic variability and amplitude.

ACPD
15, 9173–9202, 2015

Stratospheric geoengineering impacts on ENSO

C. J. Gabriel and A. Robock

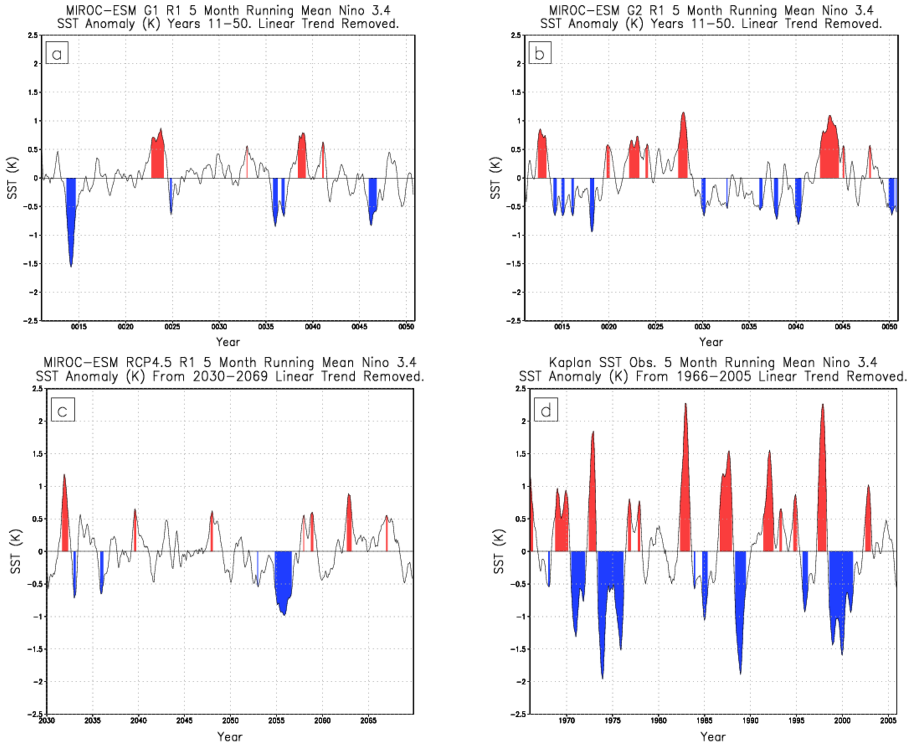

Figure 5. Niño 3.4 anomalies for MIROC-ESM. Time series of **(a)** G1, **(b)** G2 and **(c)** RCP4.5 from each model all show significantly muted variability and amplitude compared to **(d)** observations, with few, if any, warm events exceeding a 1 K anomaly. All other MIROC family experiments showed the same muted variability. Cold event amplitude is essentially muted, with no 1 K or greater departures. The inability of the MIROC-ESM to depict a plausible ENSO cycle is also seen in the MIROC-ESM-CHEM. Therefore, both sets of model output were excluded.

ACPD
15, 9173–9202, 2015

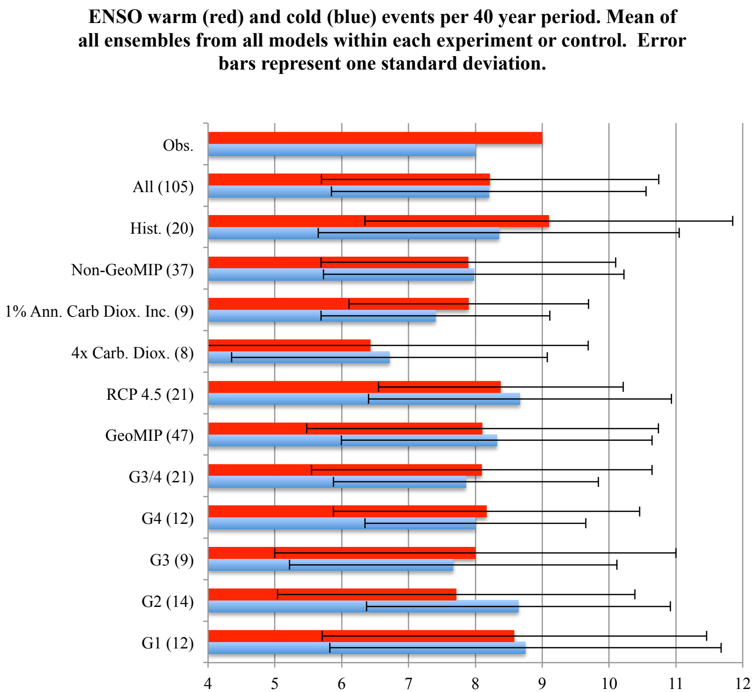

	G1 (12)	G2 (14)	G3 (9)	G4 (12)	G3/4 (21)	GeoMIP (47)	RCP 4.5 (21)	4x Carb. Diox. (8)	1% Ann. Carb Diox. Inc. (9)	Non-GeoMIP (37)	Hist. (20)	All (105)	Obs.
Warm Events	8.58	7.71	8.00	8.17	8.10	8.11	8.38	6.43	7.90	7.89	9.10	8.22	9.00
Cold Events	8.75	8.64	7.67	8.00	7.86	8.32	8.67	6.71	7.40	7.97	8.35	8.20	8.00

Figure 6. Number of ENSO warm (red) or cold (blue) events observed or simulated in the applicable 40-year comparison period for the CanESM, CSIRO, GISS, HadGEM, IPSL and MPI models. Values in parentheses are the number of ensemble members for each experiment or family of experiments. Error bars represent plus or minus one SD of ENSO events relative to the experiment mean. A table of values is provided under the graph.

ACPD
15, 9173–9202, 2015

Title Page
Abstract | Introduction
Conclusions | References
Tables | Figures
◀| |▶
◀ ▶
Back | Close
Full Screen / Esc
Printer-friendly Version
Interactive Discussion

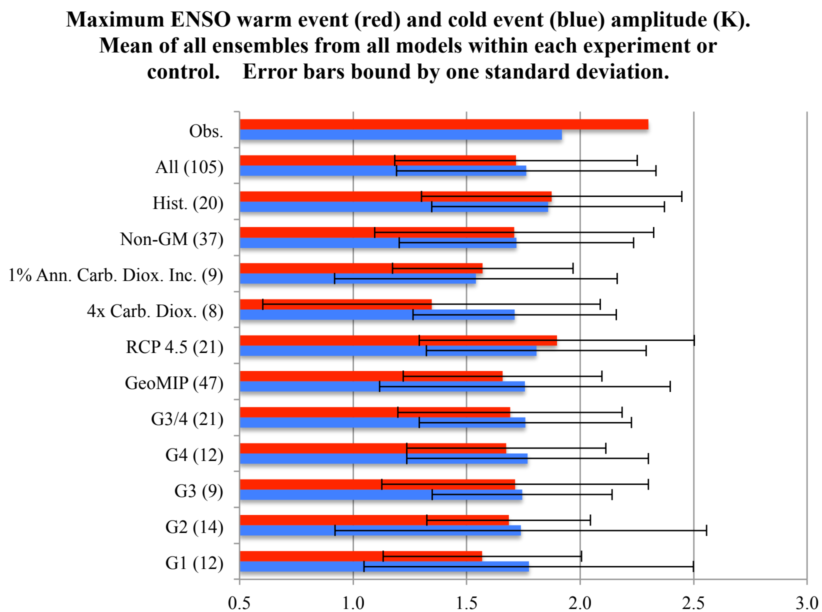

	G1 (12)	G2 (14)	G3 (9)	G4 (12)	G3/4 (21)	Geo MIP (47)	RCP 4.5 (21)	4x Carb. Diox. (8)	1% Ann. Carb. Diox. Inc. (9)	Non-GM (37)	Hist. (20)	All (105)	Obs.
Max. Warm Event. Amp. (K)	1.57	1.69	1.71	1.68	1.69	1.66	1.90	1.35	1.57	1.71	1.88	1.72	2.30
Max. Cold Event. Amp. (K)	1.77	1.74	1.74	1.77	1.76	1.76	1.81	1.71	1.54	1.72	1.86	1.76	1.92

Figure 7. Maximum amplitude of ENSO warm (red) or cold (blue) events observed or simulated in the applicable 40-year comparison period for the CanESM, CSIRO, GISS, HadGEM, IPSL and MPI models. Values in parentheses are the number of ensemble members for each experiment or family of experiments. Error bars represent plus or minus one SD of ENSO events relative to the experiment mean. A table of values is provided under the graph.

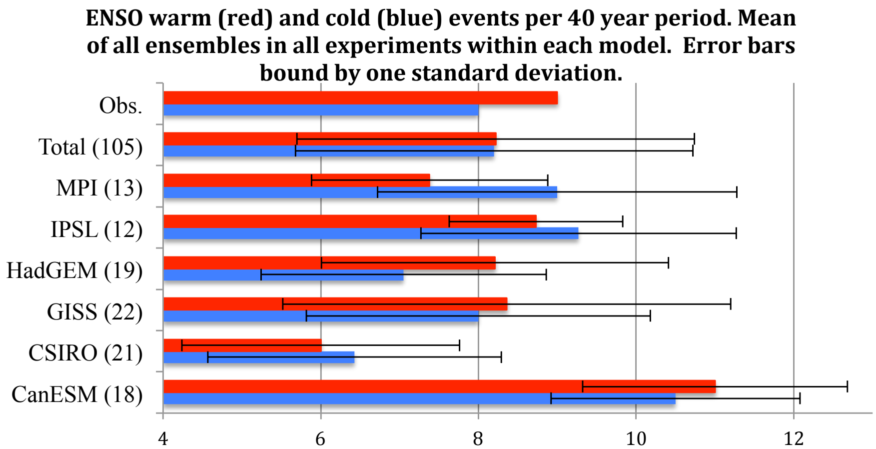

	CanESM (18)	CSIRO (21)	GISS (22)	HadGEM (19)	IPSL (12)	MPI (13)	Total (105)	Obs.
Warm Events	11.00	6.00	8.36	8.21	8.73	7.38	8.22	9.00
Cold Events	10.50	6.43	8.00	7.05	9.27	9.00	8.20	8.00

Figure 8. Number of ENSO warm (red) or cold (blue) events observed or simulated in the applicable 40-year comparison period. Values in parenthesis following *y* axis (model name) labels indicate the number of ensemble members, inclusive of all experiment designs, run by the particular model. Error bars enclose plus or minus one SD of ENSO events relative to the model mean. A table of values is provided under the graph.

ACPD
15, 9173–9202, 2015

C. J. Gabriel and A. Robock

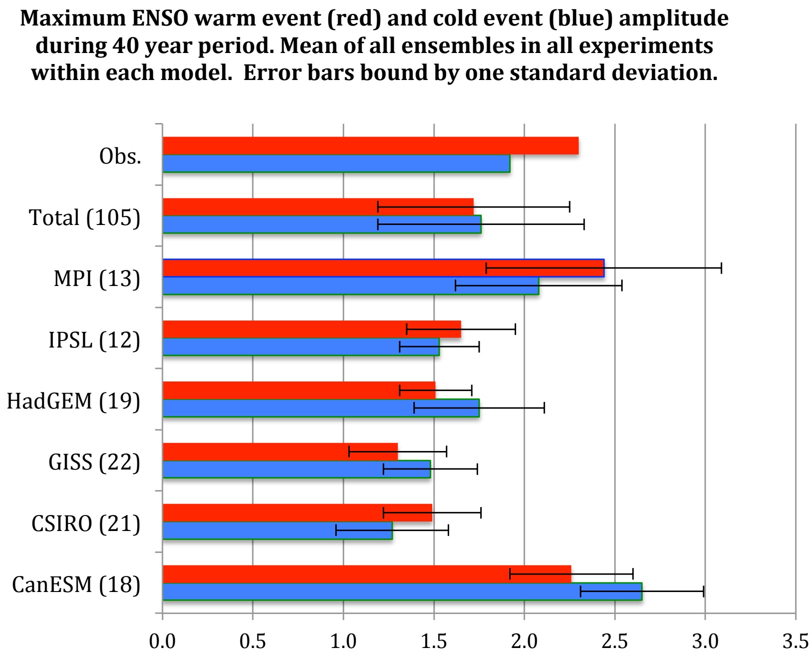

	CanESM (18)	CSIRO (21)	GISS (22)	HadGEM (19)	IPSL (12)	MPI (13)	Total (105)	Obs.
Max. Warm Amp. (K)	2.26	1.49	1.30	1.51	1.65	2.44	1.72	2.30
Max. Cold Amp. (K)	2.65	1.27	1.48	1.75	1.53	2.08	1.76	1.92

Figure 9. Maximum amplitude (K) of ENSO warm (red) or cold (blue) events observed or simulated in the applicable 40-year comparison period. Values in parenthesis following *y* axis (model name) labels indicate the number of ensemble members, inclusive of all experiment designs, run by the particular model. Error bars enclose plus or minus one SD of ENSO events relative to the model mean. A table of values is provided under the graph.

ACPD
15, 9173–9202, 2015